Int. J. Electrochem. Sci., 12 **(2017)** 2704 – 2718, doi: 10.20964/2017.04.39

International Journal of
ELECTROCHEMICAL
SCIENCE
www.electrochemsci.org

Synthesis of NiO/Activated Carbon Composites and Their Application as Electrode Materials for Capacitors

Jing-Pei Cao[1,], Shan He[1], Yan Wu[1], Xiao-Yan Zhao[1], Xian-Yong Wei[1] and Takayuki Takarada[2]*

[1] Key Laboratory of Coal Processing and Efficient Utilization (Ministry of Education), China University of Mining & Technology, Xuzhou 221116, Jiangsu, China
[2] Division of Environmental Engineering, Gunma University, 1-5-1 Tenjin-cho, Kiryu 376-8515, Japan
[*]E-mail: caojingpei@cumt.edu.cn, beyondcao@hotmail.com, beyondcao_2000@163.com

Received: 9 January 2017 / *Accepted:* 21 February 2017 / *Published:* 12 March 2017

Electrochemical capacitor (EC) based on NiO/activated carbon (AC) composite electrodes was investigated in this work to improve its electrochemical performance. NiO/AC composites were prepared as anode, while HyperCoal-based ACs were used as cathode for EC. The composites were characterized by means of X-ray diffraction and scanning electron microscopy. The porosity of HyperCoal-based ACs was characterized by N_2 adsorption-desorption analyses. The electrochemical characterization of capacitor was examined using galvanostatic charge-discharge in 1 M and 8 M KOH electrolyte solution. The results show that NiO/AC composite electrodes exhibit a good electrochemical performance with a maximum specific capacitance (C_g) of 214.48 F g^{-1} at the charge-discharge current density of 40 mA g^{-1} in 1 M KOH electrolyte. Meanwhile, the C_g increases gradually with the increase of NiO content. In addition, the C_g of EC prepared in 8 M KOH aqueous is higher than that of EC prepared in 1 M KOH aqueous until the content of NiO reaches up to 55.6%.

Keywords: electrochemical capacitor, NiO, activated carbon, composite electrodes, specific capacitance.

1. INTRODUCTION

Electrochemical capacitors (ECs), also called supercapacitors or ultracapacitors, have drawn tremendous attention as a promising energy storage device for their higher cycle life, and rapid charging-discharging than traditional batteries [1,2]. Generally, ECs can be divided into the electric double layer capacitors (EDLCs, capacitance from the charge accumulation at the electrode-electrolyte interface) and pseudocapacitors (capacitance from reversible faradaic reaction occurring at the electrode surface) depended on different energy-storage mechanisms [3,4]. Recently, various

carbonaceous materials, including activated carbons (ACs) [5-7], AC aerogels [8,9], nanotubes [10,11] and graphene [12,13] have been studied extensively as the electrode materials for EDLCs, among that ACs with high specific surface area (SSA) are considered as the promising electrode materials because of their attractive properties, such as chemical stability and relatively low cost [14,15]. HyperCoal (HPC) is an ash-free coal obtained by thermal extraction of coal via a HPC process. It has been proven to be a suitable and low-cost electrode materials of EDLCs [16,17]. However, similar to other carbon materials, EDLCs from HPC-based ACs also suffer from low energy density.

Scientists have focused much effort on investigating pseudo-capacitive transition-metal oxides to improve the power and energy densities of EDLCs [18]. Li et al. [19] found that the incorporation of metal oxide into carbon materials greatly improve the capacitance and energy density of EDLCs. Metal oxides like RuO_2 [20] and IrO_2 [21] have been investigated and demonstrated as ideal electrode materials for supercapacitors due to their great specific capacitance (C_g), whereas the high cost has limited their application. Specially, with its relatively low cost, environmental benignity and excellent electrochemical reaction, NiO has been recognized as a promising alternative candidate for electrode materials in redox ECs [22].

Many researchers investigated the incorporation of NiO into various carbon materials for ECs. Park et al. [23] reported an EC based on $Ni(OH)_2$/AC composite electrodes and the C_g value reached to 530 F g^{-1}. Ganesh et al. [24] investigated a supercapacitor based on NiO with AC as a cathode, which was shown to be a potential candidate for a supercapacitor electrode material. Yuan et al. [25] studied NiO nanoparticles on AC as electrode materials of ECs and the C_g of such materials increased from 175 to 194 F g^{-1} compared with the original pure AC.

In this study, the synthesis of NiO/AC composites and electrochemical properties of the composite electrodes are investigated. NiO/AC composites were prepared as the anode materials, and HPC-based ACs were used as cathode materials for supercapacitors. The electrochemical capacitive behavior of the NiO/AC composite electrodes was studied using the technique of galvanostatic charge-discharge tests in 1 M and 8 M KOH electrolyte solution.

2. MATERIALS AND METHODS

Table 1. The proximate and ultimate analyses (wt.%) of HPC.

Proximate analysis			Ultimate analysis (daf)				
A_d	V_d	FC_d*	C	H	N	O*	S
0.03	37.8	62.17	83.5	5.4	2.2	8.3	0.6

*: by difference; d: dry basis; daf: dry and ash free basis.

2.1. Materials

The HPC was provided by Kobe Steel, Ltd., in Japan. The production and main characteristics of the HPC were described in detail previously [26]. The property of the HPC is shown in Table1.

2.2 Preparation of NiO/AC

The AC with the SSA of 1290.67 m^2 g^{-1} was manufactured by GL Science, which was named AC-C. AC-C was firstly treated in 5 M HCl solution and stirred for 1 h to remove ash, then the AC-C was filtrated and washed with distilled water till neutral, and dried at 107 ^oC under inert atmosphere. The obtained AC was added to the $Ni(NO_3)_2$ solution, followed by stirring for 12 h after the injection of NaOH solution with a $Ni(NO_3)_2$/NaOH molar ratio of 1:2. The precipitate was washed with distilled water several times and then dried in vacuum at 140 ^oC for 8 h. The sample was obtained by calcination in inert atmosphere at the temperature range of 100-800 ^oC for 3 h.

The composites were mixed with 0.1 M HNO_3 solution, and stirred for 1 h, then the filtrate obtained from vacuum filtration was diluted with distilled water to measure concentration (1-5 ppm), solid residue was extracted by acid. Repeat the above operation. Subsequently, the total amount of nickel in the filtrate was measured using the Shimadzu AA-6400F atomic absorption method, and the ratio of nickel to AC was calculated.

The adsorption isotherm of N_2 was measured at 77 K by a BELSORP-max constant volume adsorption apparatus, and the SSA was calculated by multi-point BET method.

The structure of the composites was determined by Rigaku SmartLab X-ray diffraction (XRD) using Cu Kα radiation with a scanning range of 20-82^o. The morphology of the composites was captured by FEI XL30 ESEMFEG scanning electron microscopy (SEM).

2.3 Preparation of HPC-based ACs

The HPC was heated to 500 ^oC at a heating rate of 10 ^oC min^{-1} under Ar flow and carbonized at the prescribed temperature for 2 h. The char was mixed with KOH at a KOH/char ratio of 4, and then the mixture was activated at 500 ^oC for 2 h under Ar flow. After being cooled down to room temperature, the residue was washed with 5 M HCl and rinsed with distilled water until neutral. Subsequently, the product was dried in vacuum at 200 ^oC for 2 h. The HPC-based AC prepared by the conventional two-step activation was designated as AC-500. The AC-600 carbonized and activated at 600 ^oC was prepared in the same way.

The adsorption isotherm of N_2 was measured on the HPC-based ACs at 77 K by a constant volume adsorption apparatus (BELSORP-max), and the SSA was calculated by multi-point BET method.

2.4 Preparation of Electrode and Capacitance Measurements

The anode was prepared by mixing NiO/AC with the maximum SSA, acetylene black and polytetrafluoroethylene (PTFE) at a weight ratio of 90:9:1. And the cathode was prepared by the mixture of 87 wt.% AC (AC-C, AC-500 and AC-600 as activate material, respectively), 10 wt.% acetylene black and 3 wt.% PTFE binder. The mixture was mechanically blended and pressed onto an aluminum mesh current collector at 10 kg cm^{-2}. Then, the electrodes were dried under vacuum at 200 ^oC for 2 h. The capacitor was assembled with two electrodes using 1 M KOH aqueous and 8 M KOH

aqueous as the electrolyte, respectively. The charge-discharge measure was carried out at constant current density of 40 mA g^{-1} in the potential range of 0 to 1.5 V. The C_g was deduced from the formula:

$$C_g = 2I\mathrm{d}t/\mathrm{d}V \qquad (1)$$

where I is the discharge current density (mA g^{-1}), dt is the discharge time variation, and dV is the voltage variation in discharge.

3. RESULTS AND DISCUSSION

3.1 Structural Characterization of NiO/AC

Table 2. Characteristics of NiO/AC composites obtained at different calcination temperatures.

Sample	SSA [m^2 g^{-1}]	Pore volume [cm^3 g^{-1}]	Pore diameter [nm]
no treatment	144	0.12	3.35
100 °C Calcination	181	0.14	3.05
200 °C Calcination	210	0.17	3.16
300 °C Calcination	250	0.22	3.50
400 °C Calcination	75	0.13	6.85
500 °C Calcination	23	0.09	15.1
600 °C Calcination	12	0.07	22.5
700 °C Calcination	7	0.05	31.5
800 °C Calcination	2	0.03	53.6

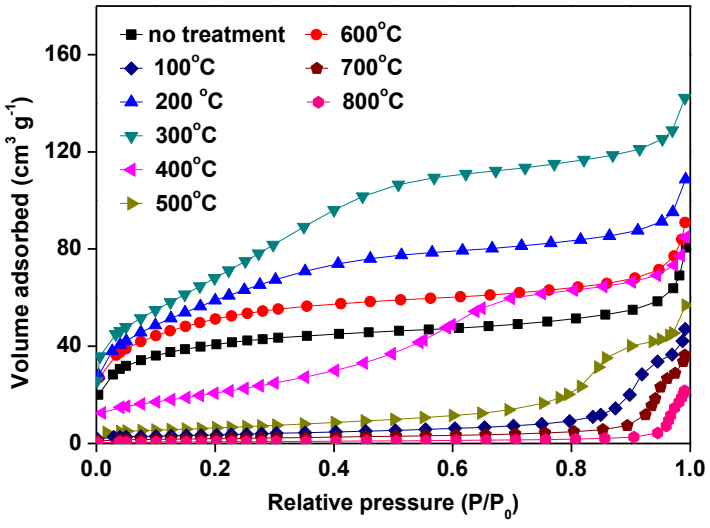

Figure 1. N_2 adsorption isotherms of the NiO/AC composites obtained at different calcination temperatures.

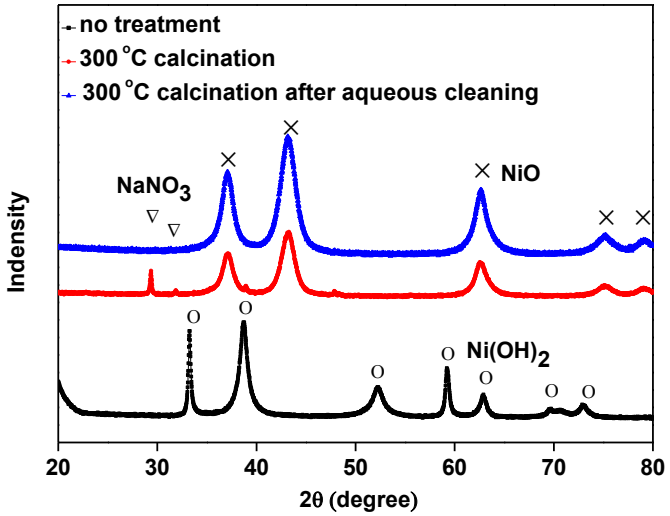

Figure 2. XRD patterns of NiO/AC composites obtained with untreated, 300 °C calcination and 300 °C calcination after aqueous cleaning.

Characteristics of NiO/AC composites obtained at different calcination temperatures ranging from 100 to 800 °C are listed in Table 2. The results show that the SSA and the pore volume increased with the increase of calcination temperature until 300 °C and then decreased when the calcination temperature was heated up to 300 °C. However, the pore diameter of the composite decreased with the increase of calcination temperature. The NiO/AC composites calcined at 300 °C exhibits the maximum SSA of 250 $m^2 g^{-1}$ and the maximum pore volume of 0.22 $cm^3 g^{-1}$, which corresponds to the adsorption isotherms in Figure 1.

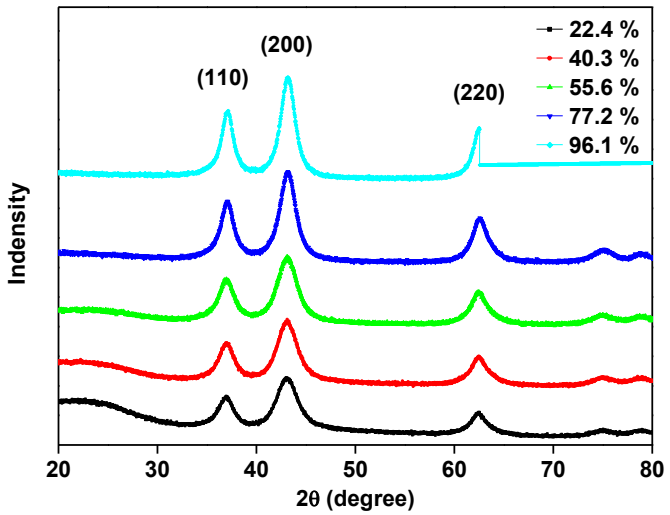

Figure 3. XRD patterns of NiO/AC composites with different NiO contents (300 °C calcination).

The XRD patterns of NiO/AC composites obtained with untreated, 300 °C calcination and 300 °C calcination after aqueous cleaning are shown in Figure 2. It can be seen that the NiO/AC composites obtained without treatment mainly contains $Ni(OH)_2$, which transfer to $NaNO_3$ and NiO under 300 °C calcination, and then after aqueous cleaning the compound is mainly NiO. The XRD

measurement confirms that NiO/AC can be obtained by calcination of the powder in inert air at 300 ^{o}C for 3 h. The content of NiO in the composite materials by calcination at 300 ^{o}C was calculated as 22.4%, 40.3%, 55.6% and 96.1%, respectively.

The XRD patterns of NiO/AC composites with different NiO contents (300 ^{o}C calcination) are shown in Figure 3. There are three broad peaks at 20~37.2^{o}, 43.2^{o} and 62.6^{o} in the wide-angle XRD patterns, corresponding to (111), (200) and (220) diffraction planes of cubic structure of NiO. This demonstrates that the calcination temperature of 300 ^{o}C was sufficient to drive to the conversion to NiO, which corresponds to the XRD of nickel compound. Furthermore, the NiO characteristic peak gradually turns to be sharper and higher with the increase of NiO content.

SEM observations of NiO/AC composites calcinated at 300 ^{o}C are shown in Figure 4. The SEM micrographs reveal that the film surface looks highly porous and fine particles structure with some overgrown clusters. The high porosity and large pore size of films are expected to result in high packing density of NiO/AC as such structure allows for easy access of the electrolyte in the redox process and facilitates transport of electrolyte ions during the rapid charge-discharge progress [27,28].

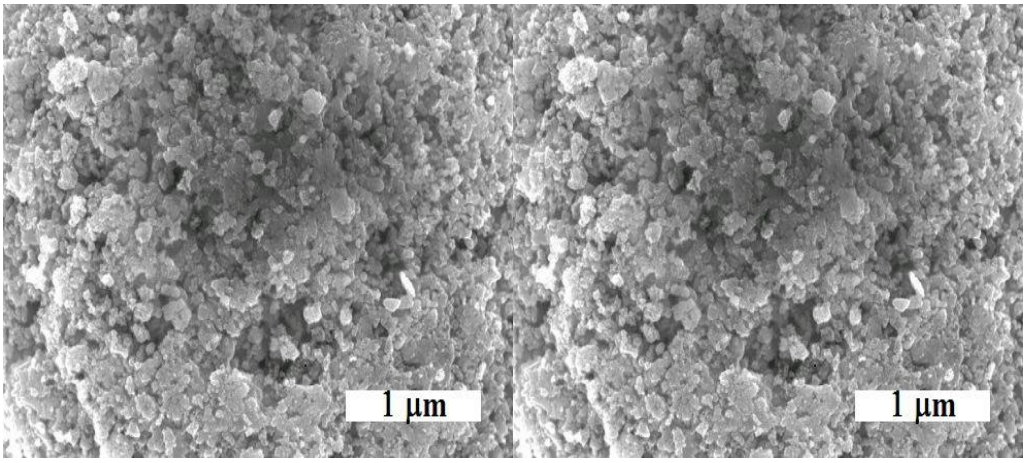

Figure 4. SEM images of NiO/AC calcinated at 300 ^{o}C.

3.2 Structural Characterization of HPC

As illustrated in Figure 5, the isotherm of ACs obtained from HPC is similar to type I according to IUPAC classification [29]. The isotherm exhibits a sharp knee at low relative pressure and horizontal adsorption plateau at high relative pressure, which shows the characteristic of micropore structure. As listed in Table 3, the SSA increases from 1296.45 m^2 g^{-1} for AC-500 to 2034.38 m^2 g^{-1} for AC-600, following by the pore volume increases from 0.58 cm^3 g^{-1} to 0.97 cm^3 g^{-1}. The results indicate that the SSA and pore structure of ACs are strongly dependent on the carbonization and activation temperatures [30,31]. There are three types of pore structures such as micro (<2 nm), meso (2–50 nm) and macro (>50 nm) pores [32]. Figure 6 exhibits the pore size distribution of ACs obtained from HPC, in which the microspores are dominant. The capacitor with the AC electrodes possess the higher SSA, can store more energy on its developed electrode/electrolyte

interface as the ACs surface provides the interface for the formation of the double layer. However, not all of the SSA is available. Only the SSA with appropriate pore size can adsorb relatively large amount of electrolyte on their wall, as a result leading to a relatively high capacitance [33,34].

Table 3. The characterization of AC-C and ACs obtained from HPC.

Sample	SSA [$m^2 g^{-1}$]	Pore volume [$cm^3 g^{-1}$]	Pore diameter [nm]
AC-C	1290.67	0.58	1.78
AC-500	1296.45	0.56	1.79
AC-600	2034.38	0.97	1.90

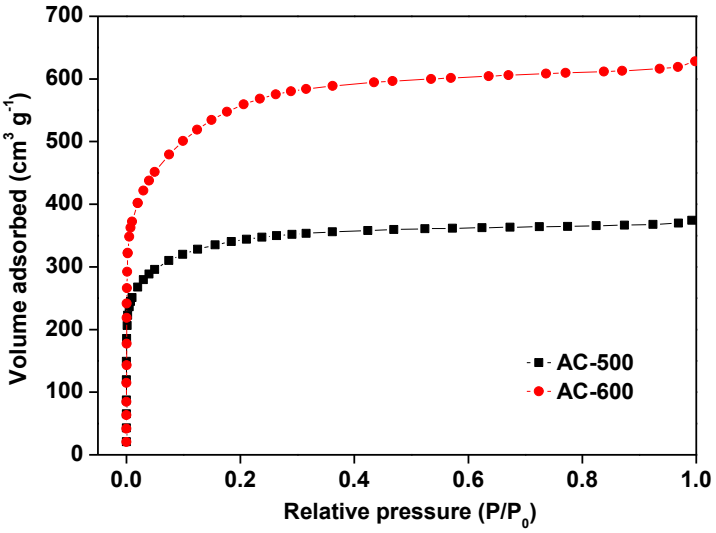

Figure 5. N_2 adsorption isotherms of ACs obtained from HPC.

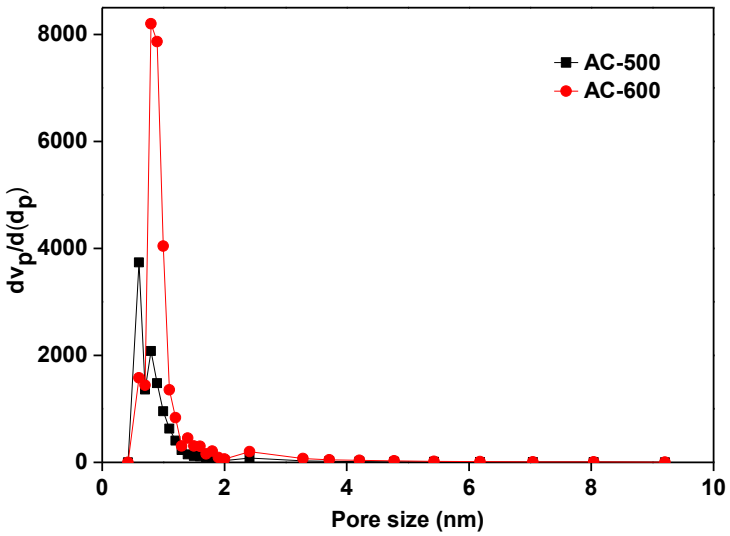

Figure 6. Pore size distribution of ACs obtained from HPC.

3.3 Electrochemical Performance of Composite Electrodes in ECs

The galvanostatic charge-discharge behavior of composite electrodes was measured at a current density of 40 mA g^{-1}. Fig. 7 shows the charge-discharge curves of composite electrodes using different cathode of AC-C, AC-500 and AC-600 and NiO/AC with the NiO content of 55.6% as anode. Fig. 8 presents the charge-discharge curves of composite electrodesusing NiO/AC with different NiO content as anode and AC-600 as cathode.

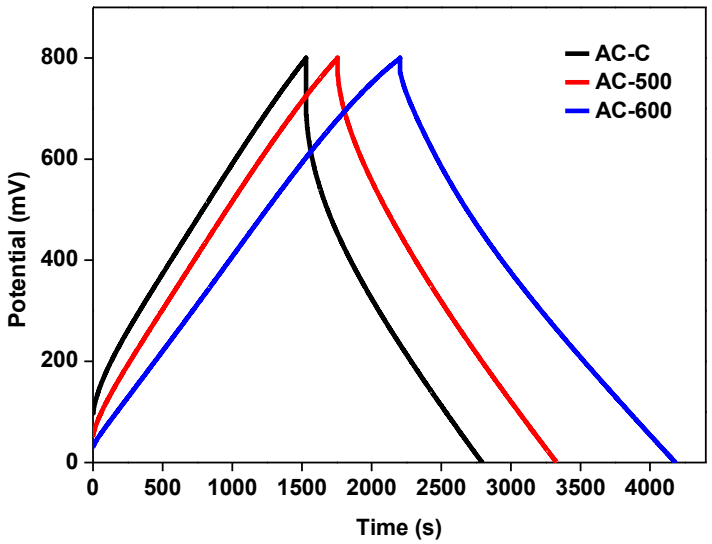

Figure 7. Charge-discharge curves of composite electrodes (anode: 55.6% NiO content, 1.0 M KOH).

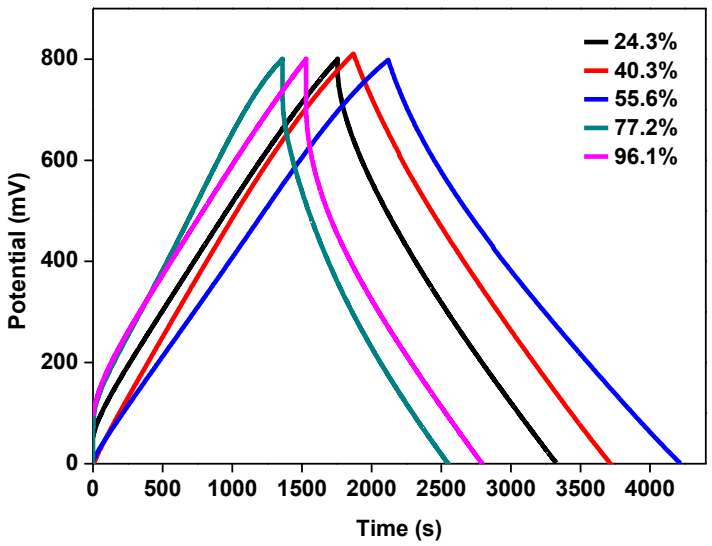

Figure 8. Charge-discharge curves of composite electrodes (cathode: AC-600, 1.0 M KOH).

It can be clearly displayed that all the curves of composite electrodes exhibit regular triangular-shapes with iR voltage drops, which is similar to the characterization of symmetrical EDLC. Besides, the constant slope of curves reveals that the composit electrode of the 55.6% NiO content was anode and the AC-600 was cathode has high capacitance, implying the existence of 55.6% of NiO results in excellent electrochemical reversibility and supercapacitive characteristics. The charge time is longer than the discharge time, suggesting a loss of capacity in this AC sample during the charge-discharge process.

The C_g of composite electrodes obtained in 1 M KOH and 8 M KOH can be calculated from the charge-discharge measure, and the results are listed in Tables 4 and 5, respectively. The higher C_g of 214.48 F g^{-1} can be obtained at a NiO content of 55.6% with AC-600 in 1 M KOH, comparing to the AC electrodes in our previous study (for two AC electrodes) [35]. The enhanced capacitance is attributed to pseudocapacitive capacitance based on Faradic redox reaction as equation (2) [36].

$$NiO + OH^- \leftrightarrow NiOOH + e^- \quad (2)$$

The charge-discharge mechanism in alkaline aqueous solution is based on the quasi-reversible faradaic redox process of Ni^{2+} to Ni^{3+} between the interfaces of electrode/electrolyte. For the electrochemical redox between the NiO particles and KOH electrolyte, the surface Faradaic reaction of Ni^{2+} to Ni^{3+} occurs at the surface of NiO, while the reverse Faradaic reaction of Ni^{3+} to Ni^{2+} occurs during reduction [37]. Moreover, the formation of NiOOH can improve electronic conductivity, which is more efficient to enhance the capacitive current response [38].

Table 4. The C_g of composite electrodes obtained in 1 M KOH.

Sample	C_g [F g^{-1}]				
	24.3%	40.3%	55.6%	77.2%	96.1%
AC-C	136.18	150.38	182.38	109.80	108.80
AC-500	153.21	164.37	193.51	102.25	121.18
AC-600	172.09	176.52	214.48	124.94	161.82

Table 5. The C_g of composite electrodes obtained in 8 M KOH.

Sample	C_g [F g^{-1}]				
	24.3%	40.3%	55.6%	77.2%	96.1%
AC-C	169.30	184.10	199.40	104.81	103.86
AC-500	168.73	186.15	205.06	101.42	115.68
AC-600	196.62	210.54	235.50	119.26	154.47

Many efforts are reported to optimize NiO morphologies and their composites with carbon structure/metals to enable a high C_g of supercapacitors. Table 6 shows part of the research using NiO nanostructure and their composites for application as a supercapacitor electrode, which is comparable with the results of the NiO/AC composite. It can be seen that the C_g reported are depended on experimental condition of current density or electrolyte, and NiO nanostructure and their composites

with carbon structures/metals are appropriate as electrode materials for a high performance of supercapacitors. Moreover, the synthesis of NiO/AC composite by the soft chemical approach is available for the electrode material and is effective for the high capacitance of capacitors.

Table 6. Summary of research on the use of NiO nanostructure and their composites with carbon structures/metals for application as a supercapacitor electrode.

Morphology	Method of synthesis	C_g (F g^{-1})	Current density	Electrolyte	Ref.
Porous thin film	Chemical bath depositon	51.79	1 mA cm^{-1}	1M KOH	[39]
NiO nanotubes	Hydrothermal	701	0.5 A g^{-1}	KOH	[40]
Porous NiO nanowall arrays	Direct synthesis	236	13.35 A g^{-1}	no data available	[41]
NiO/carbon nanaotubes	Chemical bath depositon	162.41	0.5 mA g^{-1}	1 M KOH	[42]
Graphene/NiO composite	Hydrochermal	617	1 A g^{-1}	5 M NaOH	[43]
NiO/Ni composite	Simple reduction method	789	0.5 A g^{-1}	No data available	[44]
Co/NiO core shell nanowire	Hydrogen Reduction+chemical bath depositon	956	2 A g^{-1}	No data available	[45]
Ni-(Cu)	Electrodepositon	428	No data available	1 M KOH	[46]

Figure 9 shows the effect of NiO content on the capacitance of composite electrodes prepared using the AC-C as the cathode in 1 M KOH. It can be seen that the C_g slightly increased with the increase of NiO content from 24.3% to 55.6%, and then decreased dramatically when the NiO content reaches to 77.2%. This trend suggests that the incorporation of NiO into AC can improve the capacitance, which is mainly due to the quasi-reversible redox process occurs at the surface of NiO [47]. However, direct linear relationship between the measured capacitance and NiO content were not found in this work. This phenomenon could be explained by the isolation of porous core network due to large amount of NiO generated on the electrode surface layer. Besides, more NiO content can lead to the increase of the resistivity of electrode, as a result making the weak capacitive behavior [48].

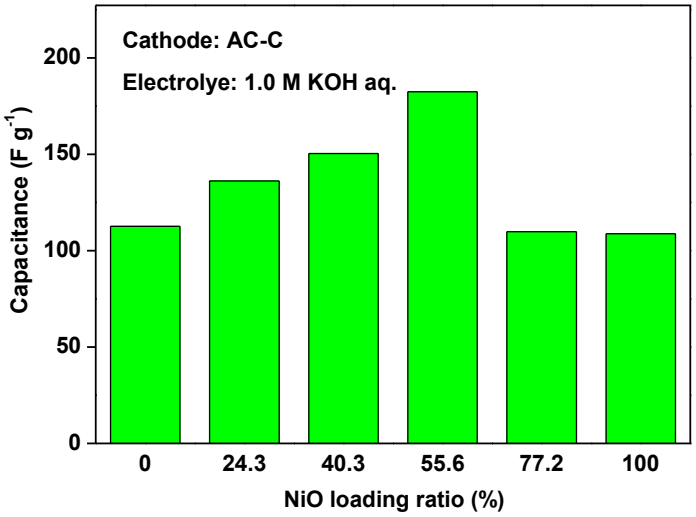

Figure 9. The effect of NiO content on the C_g of the NiO/AC.

It is obvious that the C_g of ACs obtained from HPC is higher than that of AC-C as shown in Figure 10, which is mainly contributed to the production of pseudo-capacitance with the introduction of NiO. At the same time, ACs with a high SSA can provide a large double-layer capacitance, leading to a high capacitance of composite electrodes. Lee et al. [49] reported that as redox reaction occurs at the interface of electrolyte and NiO particles, high C_g can be obtained under conditions of high SSA of active materials and narrow pore distribution with many channels for diffusion of OH^- ions.

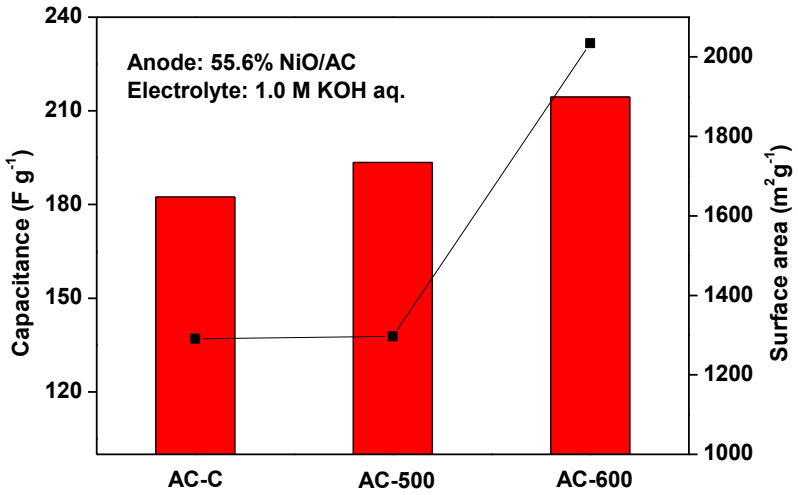

Figure 10. Type of cathode material (1.0 M KOH).

It should be noticed that the C_g of AC-600 is higher than that of AC-500 regardless of the NiO content. It can be explained that AC-600 has a high SSA of 2034.38 m^2 g^{-1} which can offer more available interface to store energy. ACs with large SSA and suitable pore size distribution are beneficial for the accessibility of electrolytes to electrochemically active sites and fast diffusion of electrolyte ions during rapid charge-discharge process [50-52]. Similarly, the highest C_g is obtained at NiO content of 55.6% in 8 M KOH aqueous regardless of the cathode materials as listed in the Table 5 and Figure 11. The C_g of AC-600 is higher than that of AC-C and AC-500. Apparently, the change of C_g of supercapacitors is irregular because of the partial utilization of the SSA, which is attributed to the restriction accessibility of electrolyte ions to the pores or the incomplete wet of ACs [17].

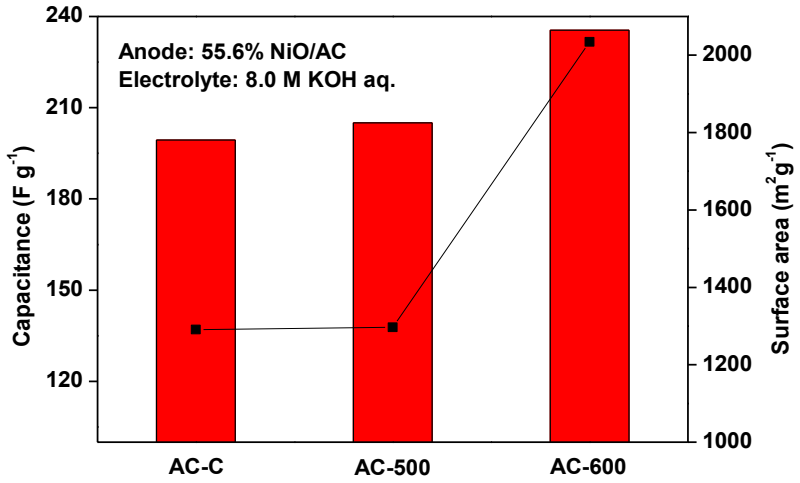

Figure 11. Type of cathode material.

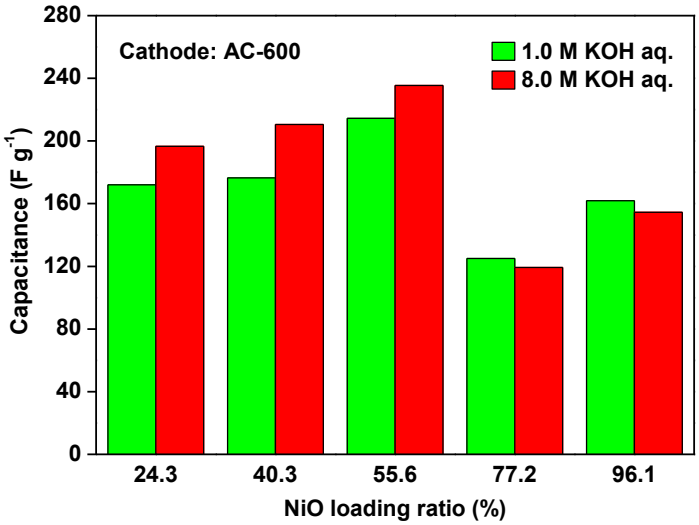

Figure 12. Effect of concentration of KOH aqueous on the C_g of the NiO/AC.

It can be easily observed in Figure 10 that the C_g of AC-600 in 8 M KOH is higher than that of in 1 M KOH when the NiO content lower than 55.6%. A high C_g of 235.50 F g^{-1} is obtained at 55.6% NiO content with AC-600 (2034.38 m^2 g^{-1}) as the cathode.

However, when the NiO content is higher than 55.6%, the C_g of supercapacitors in 1 M KOH is lower than that in 8 M KOH. The electrical conductivity of the solution increases obviously with the increase of the electrolyte concentration. The electric conductivity decreases when the concentration of electrolyte exceeds a certain range. The increase of electrical conductivity may lead to the decrease of the resistance of the ions diffusion in the charge-discharge process and thus cause the increase of the capacitance [53].

4. CONCLUSION

The C_g of composite electrode was a combination of double-layer capacitance and pseudo-capacitance. The supercapacitor based on the NiO/AC composite electrodes exhibits a stable charge-discharge characteristic. With 1 M KOH aqueous solution as the electrolyte, supercapacitor electrode based on NiO/AC composite materials exhibits a high C_g of 214.48 F g^{-1} at the current density of 40 mA g^{-1} in the potential range of 0-1.5 V. The composite electrodes with high capacitance performance can remarkably enhance the energy density of pseudocapacitors, and promote the wide utilization of capacitors as energy storage devices.

ACKNOWLEDGEMENTS
This work was subsidized by the Fundamental Research Funds for the Central Universities (China University of Mining & Technology, Grant 2015QNA18), National Natural Science Foundation of China (Grants 21676292), Natural Science Foundation of Jiangsu Province (BK20151141) and the Priority Academic Program Development of Jiangsu Higher Education Institutions.

References

1. Q. L. Chen, K. H. Xue, W. Shen, F. F. Tao, S. Y. Yin and W. Xu, *Electrochim. Acta*, 49 (2004) 4157.
2. Z. H. Feng, R. S. Xue and X. Shao, *Electrochim. Acta*, 55 (2010) 7334.
3. L. J. Yan, X. L. Niu, W. C. Wang, X. B. Li, X. H. Sun, C. J. Zheng, J. W. Wang and W. Sun, *Int. J. Electrochem. Sci*., 11 (2016) 1738.
4. C. Peng, X. B. Yan, R. T. Wang, J. W. Lang, Y. J. Ou and Q. J. Xue, *Electrochim. Acta*, 87 (2013) 401.
5. X. J. He, P. H. Ling, M. X. Yu, X. T. Wang, X. Y. Zhang and M. D. Zheng, *Electrochim. Acta*, 105 (2013) 635.
6. L. L. Ding, B. Zou, H. Q. Liu, Y. N. Li, Z. C. Wang, Y. Su, Y. P. Guo and X. F. Wang, *Chem. Eng. J*., 225 (2013) 300.
7. M. S. Balathanigaimani, W. G. Shim, M. J. Lee, C. Kim, J. W. Lee and H. Moon, *Electrochem. Commun.*, 10 (2008) 868.
8. D. Liu, J. Shen, N. P. Liu, H. Y. Yang and A. Du, *Electrochim. Acta*, 89 (2013) 571.
9. S. H. Kwon, E. Lee, B. S. Kim, S. G. Kim, B. J. Lee, M. S. Kim and J. C. Jung, *Curr. Appl. Phys.*, 14 (2014) 603.

10. E. Frackowiak, S. Delpeux, K. Jurewicz, K. Szostak, D. Cazorla-Amoros, F. Beguin, *Chem. Phys. Lett.*, 361 (2002) 35.
11. S. H. Lee, Y. S. Park, K. H. An, S. J. Kang and M. Huh, *Carbon Lett*., 12 (2011) 102.
12. X. Du, P. Guo, H. H. Song and X. H. Chen, *Electrochim. Acta*, 55 (2010) 4812.
13. A. Davies and A. Yu, *Can. J. Chem. Eng*., 89 (2011) 1342.
14. J. Wang, M. M. Chen, C.Y. Wang, J. Z. Wang and J. M. Zheng, *J. Power Sources*, 196 (2011) 550.
15. J. W. Lang, X. B. Yan, X. Y. Yuan, J. Yang and Q. J. Xue, *J. Power Sources*, 196 (2011) 10472.
16. K. Koyano, T. Takanohashi and I. Saito, *Energy Fuels*, 23 (2009), 3652.
17. X. Y. Zhao, S. S. Huang, J. P. Cao, X. Y. Wei, K. Magarisawa and T. Takarada, *Fuel Process.Technol*., 125 (2014) 251.
18. X. H. Xia, J. P. Tu, Y. J. Mai, R. Chen, X. L. Wang, C. D. Gu and X. B. Zhao, *Chem. Eur. J*., 17 (2011) 10898.
19. H. F. Li, Y. F. Li, R. D. Wang and R. Cao, *J. Alloys Compd.*, 481 (2009) 100.
20. C. C. Liu, D. S. Tsai, D. Susanti, W. C. Yeh, Y. S. Huang and F. J. Liu, *Electrochim. Acta*, 55 (2010) 5768.
21. Y. M. Chen, C. A. Chen, Y. S. Huang, K. Y. Lee and K. K. Tiong, *J. Alloys Compd*., 487 (2009) 659.
22. M. Yang, J. X. Li, H. H. Li, L.W. Su, J. P. Wei and Z. Zhou, *Phys. Chem. Chem. Phys*., 14 (2012) 11048.
23. J. H. Park, O. K. Park, K. H. Shin, C. S. Jin and J. H. Kim, *Electrochem. Solid-State Lett.*, 5.2 (2002) H7.
24. V. Ganesh, S. Pitchumani and V. Lakshminarayanan, *J. Power Sources*, 128 (2016) 1523.
25. G. H. Yuan, Z. H. Jiang, A. Aramata and Y. Z. Gao, *Carbon*, 43 (2005) 2913.
26. N. Okuyama, N. Komatsu, T. Shigehisa, T. Kaneko and S. Tsuruya, *Fuel Process. Technol.*, 85 (2004) 947.
27. U. M. Patil, R. R. Salunkhe, K. V. Gurav and C. D. Lokhande, *Appl. Surf. Sci.*, 255 (2008) 2603.
28. W. G. Pell and B. E. Conway, *J. Electroanal. Chem*., 500 (2001) 121.
29. K. Kierzek, E. Frackowiak, G. Lota, G. Gryglewicz and J. Machnikowski, *Electrochim. Acta*, 49 (2004) 515.
30. O. Ioannidou and A. Zabaniotou, *Renew. Sust. Energ. Rev*., 11 (2007) 1966.
31. L. Wei and G. Yushin, *Nano Energy*, 1 (2012) 552.
32. S. Mitani, S. I. Lee, S. H. Yoon, Y. Korai and I. Mochida, *J. Power Sources*, 133 (2004) 298.
33. H. C. Chang, H. Y. Chang, W. J. Su, K. Y. Lee and W. C. Shin, *Appl. Surf. Sci.*, 258 (2012) 8599.
34. D. Qu and H. Shi, *J. Power Sources*, 74 (1998) 99.
35. X. Y. Zhao, S. S. Huang, J. P. Cao, S. C. Xi, X. Y. Wei, J. Kamamoto and T. Takarada, *J. Anal. Appl. Pyrolysis*, 105 (2014) 116.
36. F. Cao, G. X. Pan, X. H. Xia, P. S. Tang and H. F. Chen, *J. Power Sources*, 264 (2014) 161.
37. Y. Z. Zheng, H. Y. Ding and M. L. Zhang, *Mater. Res. Bull*., 44 (2009) 403.
38. F. B. Zhang, Y. K. Zhou and H. L. Li, *Mater. Chem. Phys.*, 83 (2004) 260.
39. A. I. Inamdar, Y. Kim, S. M. Pawar, J. H. Kim, H. Im and H. Kim, *J. Power Sources*, 196 (2011) 2393.
40. F. Lei, T. Le and G. Rong, *Cryst. Eng. Commun*., 21 (2011) 7246.
41. J. H. Zhu, J. Jiang, J. P. Liu, R. M. Ding, H. Ding and Y. M. Feng, G. M. Wei and X. T. Huang, *J. Solid State Chem*., 184 (2011) 578.
42. H. Y. Chang, H. C. Chang and K. Y. Lee, *Vacuum*, 87 (2013) 164.
43. Y. M. Chen, Z. D. Huang, H. Y. Zhang, Y. T. Chen, Z. D. Cheng, Y. B. Zhong, Y. D. Ye and X. L. Lei, *Int. J. Hydrogen Energ*., 39 (2014) 16171.
44. M. M. Liu, J. Chang, J. Sun and L. Gao. *RSC Adv*., 3 (2013) 8003.
45. G. X. Pan, X. H. Xia, F. Cao, P. S. Tang and H. F. Chen, *Electrochem. Commun.*, 34 (2013) 146.
46. L. Persano, A. Camposeo, C. Tekmen and D. Pisignano, *Macromol. Mater. Eng*., 298 (2013) 504.

47. Y. Y. Yang, Z. A. Hu, Z. Y. Zhang, F. H. Zhang, Y. J. Zhang, P. J. Liang and H. Y. Wu, *Mater. Chem. Phys.*, 133 (2012) 363.
48. C. D. Wang, J. L. Xu, M. F. Yuen, J. Zhang, Y. Y. Li, X. F. Chen and W. J. Zhang, *Adv. Funct. Mater.*, 24 (2014) 6372.
49. J. W. Lee, T. Ahn, J. H. Kim, J. M. Ko and J. D. Kim, *Electrochim. Acta*, 56 (2011) 4849.
50. H. Jiang, P. S. Lee and C. Li, *Energ. Environ. Sci.*, 6 (2013) 41.
51. B. Xu, F. Wu, R. J. Chen, G. P. Cao, S. Chen, Z. M. Zhou and Y. S. Yang, *Electrochem. Commun.*, 10 (2008) 795.
52. L. Yang, H. Li, H. Z. Liu and Y. Y. Zhang, *Int. J. Electrochem. Sci.*, 12 (2017) 1.
53. L. D. Feng, Y. F. Zhu, H. Y. Ding and C. Y. Ni, *J. Power Sources*, 267 (2014) 430.